ACS Photonics

Article

pubs.acs.org/journal/apchd5

Broadband Absorption Enhancement in Solar Cells with an Atomically Thin Active Layer

Jessica R. Piper*,† and Shanhui Fan*,‡

†Exponent, Electrical Engineering Practice, Menlo Park, California 94025, United States

‡Gintzon Laboratory, Department of Electrical Engineering, Stanford University, Stanford, California 94305, United States

ABSTRACT: We numerically demonstrate broadband absorption enhancement in the visible in monolayer MoS_2 placed on a photonic crystal slab, backed by a perfect electric conductor mirror. The absorption enhancement arises from interaction between the MoS_2 and the guided resonances of the photonic crystal slab. Through consideration of light trapping theory and parametric studies of the design parameters, it is shown that the optimal photonic crystal slab has a grating period that is *subwavelength* to most of the frequency region of interest, has *large* air holes, and is *thin*. The optimal design features an average absorption of 51% at normal incidence in the visible above the band gap of MoS_2 (400−690 nm) and is less than 100 nm thick. We also comment on the angular response of the optimal device.

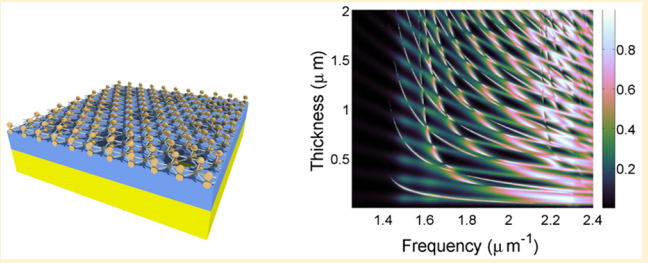

KEYWORDS: *MoS_2, transition metal dichalcogenides, photonic crystal, critical coupling, guided resonance, absorption enhancement, solar cells, Fano resonance*

Over the past decade, there has been a growing interest in the optics of atomically thin materials.[1] In particular, the last several years have seen a flurry of studies on the transition metal dichalcogenides (TMDCs) MoS_2 and WSe, which in their monolayer form are direct band gap semiconductors.[2−5] Having a direct band gap opens up many exciting possibilities for optoelectronic devices with an atomic-scale dimension. Recently, TMDC-based photodetectors,[6,7] solar cells,[8] LEDs,[9] and optically pumped lasers[10] have been demonstrated.

TMDCs can have single-pass absorption of 10−20% in the wavelength range above the band gap. While this is remarkably high for a single atomic layer, for applications such as solar cells and photodetectors this absorption is insufficient for high-performance devices. For solar cell applications, moreover, enhancement of absorption over the entire wavelength range above the band gap is desirable.

In this paper, we consider the use of resonances in photonic crystal slabs for broadband enhancement of above-band-gap absorption in single-layer MoS_2. The schematic of the configuration considered in this paper is shown in Figure 1a, where a single layer of MoS_2 is placed on top of a photonic crystal slab that sits on a mirror. Recently, there has been a great deal of interest in studying the interaction of 2D materials with engineered nanostructures.[11−19] We have previously proposed[20,21] and demonstrated[22] the use of guided resonance in photonic crystal slabs for absorption enhancement in graphene, another monolayer two-dimensional material. However, refs 20−22 focus on critical coupling as the absorption-enhancement mechanism, which results in relatively narrow-band performance. In contrast, here we show that, with proper design, the use of multiple resonances can lead to absorption enhancement over the entire frequency range above the band gap of MoS_2. For normally incident light, our optimal structure shows an average absorption of 51% over the visible spectrum, which is a significant enhancement over the average single-pass absorption of MoS_2 of approximately 10% in the same spectral range. Due to the 90° rotational symmetry of the photonic crystal resonator used, the two polarizations are degenerate at normal incidence. We also account for the performance of our absorption enhancement scheme with light trapping theory.

The remainder of the paper is organized as follows. In the Theoretical Background section, we briefly review the properties of the resonances of the photonic crystal slab that we use for the absorption enhancement, as well as the theory of broadband light trapping using multiple resonances. In the Design Parameter Study section, we discuss the optimal structure. We illustrate the physics of the optimal structure by examining the performance of the structure as a function of its geometric parameters. In the Angular Response section, we discuss the angular response of the optimal structure. We summarize our results in the Conclusion section.

THEORETICAL BACKGROUND

To enhance absorption, the common approach is to utilize resonances.[23] In the visible wavelength range, monolayer TMDCs do not possess strong resonant behavior. Therefore, we place the TMDC layer on a photonic crystal slab, in order to utilize the resonances of the photonic crystal slab. The

Received: September 16, 2015
Published: March 10, 2016

DOI: 10.1021/acsphotonics.5b00510
ACS Photonics 2016, 3, 571−577

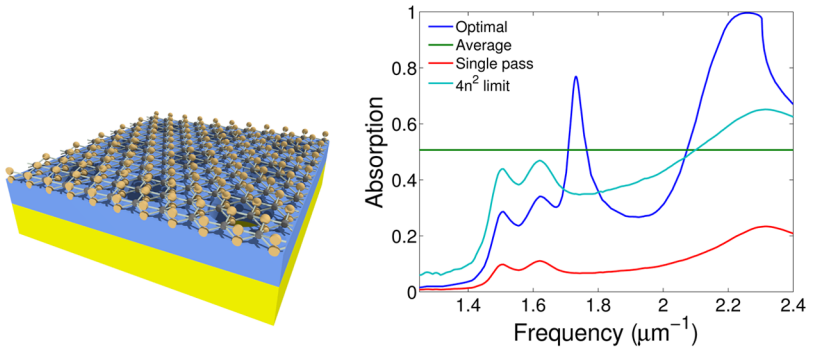

Figure 1. (a) Schematic of absorption enhancement system for MoS_2. The system uses a perfect electric conductor mirror (yellow) and a high-index dielectric photonic crystal slab (blue). The monolayer MoS_2 is the honeycomb fishnet on top. (b) Absorption spectrum for the locally optimal structure, along with the single-pass absorption of MoS_2 and the absorption as predicted by the $4n^2$ limit.

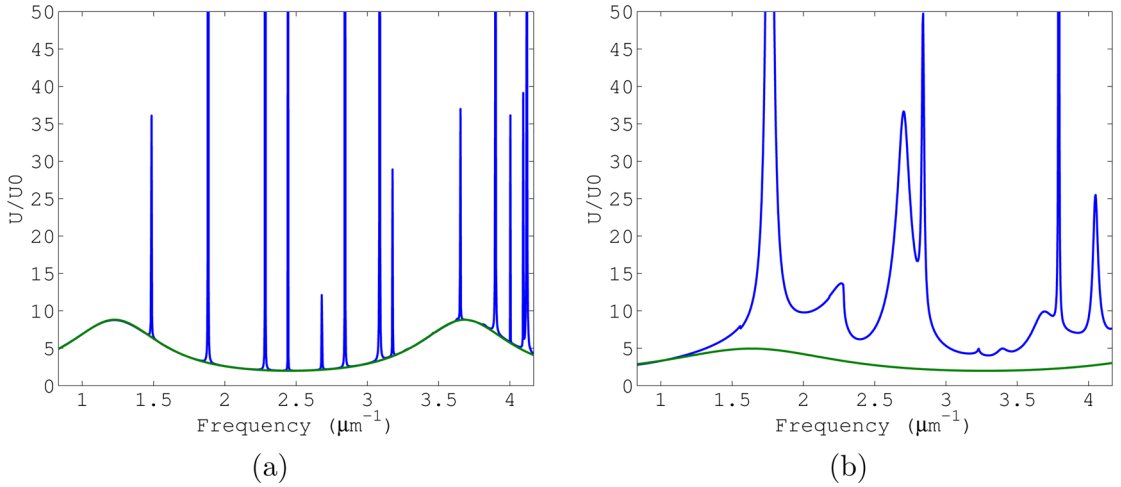

Figure 2. Energy density enhancement for a photonic crystal slab backed by a PEC mirror (blue curves), compared to that in an unpatterned dielectric slab on a PEC mirror (green curves). (a) The photonic crystal slab has $\Lambda = 438$ nm, $r = 0.043\Lambda$, $d = 97$ nm, $n = 2.1$. The homogeneous dielectric slab has $d = 97$ nm, $n = 2.1$. The high-Q guided resonances are superimposed on top of a Fabry–Perot background. (b) The photonic crystal slab has the same period and thickness, but $r = 0.43\Lambda$, while the homogeneous dielectric slab has $d = 97$ nm and $n = 1.6$.

absorption enhancement in our device is due to the interaction of MoS_2 with two types of resonances, a Fabry–Perot background and the photonic crystal guided resonances, so we examine each of them in turn.

An unpatterned dielectric slab on a mirror exhibits a series of constant-Q resonances that are evenly spaced in frequency; we refer to these as the Fabry–Perot background, since such a system forms a simple type of Fabry–Perot resonator. For a slab of thickness d and index n on a mirror, the resonances will be periodically spaced in frequency at $\omega = (2m + 1)c\pi/2nd$, with m an integer; the line width of the resonances is constant at $\omega'' = -c \log R/4nd$, where R is the fraction of power reflected at an air–dielectric interface.

In addition to the Fabry–Perot background, the photonic crystal slab exhibits guided resonances, which arise from coherent scattering by the periodic pattern of air holes. Guided resonances are quasi-bound optical states that can be excited by light incident from free space.

We use the average energy density enhancement U/U_0 in the (homogeneous or patterned) slab as an indicator of resonant behavior. This dimensionless quantity indicates the enhancement in the average energy density inside the slab (U) as compared to the energy density in the incident wave (U_0). On-resonance, the slab has significant energy storage, and off-resonance it does not.

In Figure 2a, we see the energy density enhancement in a photonic crystal slab ($n = 2.1$, appropriate for Ta_2O_5) with small air holes backed by a PEC mirror (blue curve), along with the corresponding energy density enhancement for an unpatterned dielectric slab with the same thickness on a PEC mirror (green curve). The first two Fabry–Perot resonances, at $\pi c/2nd$ or 1.22 μm^{-1} and $3\pi c/2nd$ or 3.68 μm^{-1}, are clearly visible in Figure 2a. On top of this Fabry–Perot background are superimposed a number of high-Q Lorentzian-like contributions from the guided resonances.

Figure 2b shows corresponding curves for a photonic crystal slab with large air holes (blue) and a homogeneous dielectric slab with a reduced effective index (green). As we increase the size of the holes in the photonic crystal slab, the leakage rates of the guided resonances go up and their quality factors go down. The resonances begin to overlap each other and may constructively interfere to create a high background field enhancement. Further, as we remove material from the slab, its effective index decreases, so that we calculate the Fabry–Perot background using a slab with the original thickness but a reduced refractive index. In Figure 2b the green curve is

DOI: 10.1021/acsphotonics.5b00510
ACS Photonics 2016, 3, 571–577

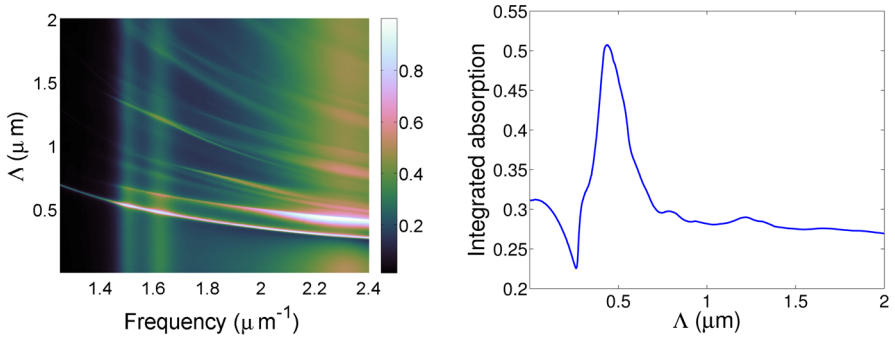

Figure 3. (a) Absorption as a function of frequency and photonic crystal slab period Λ, for fixed thickness d = 95 nm and normalized radius r = 0.431Λ. (b) Integrated absorption as a function of photonic crystal slab period Λ.

calculated using a slab with n = 1.6. The blue and green curves match well for low frequencies, but the constructive interference between the multiple guided resonances leads to an enhanced background energy density for the patterned slab as opposed to the unpatterned slab; this background contributes significantly to the broadband absorption enhancement in our device.

To account for the features of light trapping in the structure, we use the statistical temporal coupled mode theory formalism.[24] Coupled mode theory is useful for analyzing resonant systems where direct and resonant reflections and transmissions interfere coherently. In particular, coupled mode theory has been useful for discussing the guided resonances of photonic crystal slabs.[25] In this analysis, each incoming or outgoing plane wave with a fixed $k_{\|}$ and frequency constitutes a *channel*. These waves interact with the resonances (hereafter, *modes*) of the photonic crystal slab. We can characterize each mode by its central frequency ω_0, its external leakage rate γ_e, and its intrinsic loss rate γ_i. (Note that in this paper the loss is due to a thin lossy layer next to the lossless photonic crystal slab, rather than a photonic crystal slab that is made of a lossy material.) The total absorption in a lossy photonic crystal system will include contributions from each guided resonance, as well as a background term that looks like the absorption of a lossy, unpatterned slab with an effective dielectric constant.

We apply coupled mode theory to a resonator with M resonant modes and N channels. Consider a frequency range ω to $\omega + \Delta\omega$ that contains multiple modes. Assuming that each mode in this frequency range leaks equally to each of the channels at the rate γ_e and that the intrinsic loss rate γ_i of every mode is equal, it can be shown that the spectrally averaged absorption within the frequency range is[24]

$$A = \frac{2\pi}{\Delta\omega} \sum_{\text{modes}} \frac{\gamma_i}{N + \gamma_i/\gamma_e} \tag{1}$$

where the summation is over all modes in the frequency range $[\omega, \omega + \delta\omega]$. This sum achieves its maximum in the case where all the resonances are *overcoupled* ($\gamma_e \gg \gamma_i$), in which case we have

$$A = \frac{2\pi\gamma_i}{\Delta\omega}\frac{M}{N} \tag{2}$$

Furthermore, it can be shown from a statistical physics argument that the broadband absorption is maximized when all the leakage rates are equal, indicating that eq 2 is an upper bound on the absorption in a real system.[26] For a thick film with Lambertian (random) texturing backed with a mirror, it can further be shown that

$$A \le \frac{\alpha d}{\alpha d + 1/4n^2} \tag{3}$$

where αd is the single-pass absorption of the lossy film. For small loss, this expression reduces to $A \le 4n^2\alpha d$. This result reproduces the so-called Yablonovitch limit on absorption enhancement, originally derived from a combination of statistical mechanics and ray optics.[27] While the Yablonovitch derivation assumes a thick film ($d \gg \lambda_{max}$), this result was later extended to the case of thin lossy films.[28]

A caveat is in order when discussing the Yablonovitch limit. First, the assumption that the single-pass absorption in a thin film is given by αd is only true for materials with small absorption and negligible reflection. For films thick enough to act as etalons, the absorption is an oscillatory function of thickness or wavelength. On the other hand, for very thin films with strong absorption ($n \approx k$), one can derive using a sheet conductance model that the single-pass absorption at normal incidence is $n\alpha d$. In particular, MoS_2 has strong absorption, so when we refer to its single-pass absorption in this article, we mean the observed fraction of incident light absorbed by a monolayer of MoS_2 in air, rather than the smaller number that would be calculated from αd. Likewise, in applying the Yablonovich $4n^2$ limit, we use the observed single-pass absorption rather than αd.

DESIGN PARAMETER STUDY

Consideration of the light trapping theory reveals three fundamental design rules for our broadband absorption enhancement system. We expect the photonic crystal slab periodicity to be *subwavelength* to most of the frequency region of interest, reducing the number of channels N to 1 at most frequencies.[24] Further, the photonic crystal slab will have *large* air holes, increasing the external leakage rate γ_e.[24] Finally, and (perhaps counterintuitively) the photonic crystal slab will be *thin*. In the remainder of this section we show how these design rules are reflected in our optimal design and examine each of the rules in turn to study the behavior of the optimal design as two parameters are held constant and the third is swept.

Optimal Design. The schematic of our optimal device is shown in Figure 1a. Our structure features an average absorption of 51% over the visible spectrum (400−700 nm), surpassing the Yablonovich $4n^2$ limit, as derived for a Lambertian absorber. These spectra are shown together in

DOI: 10.1021/acsphotonics.5b00510
ACS Photonics 2016, 3, 571−577

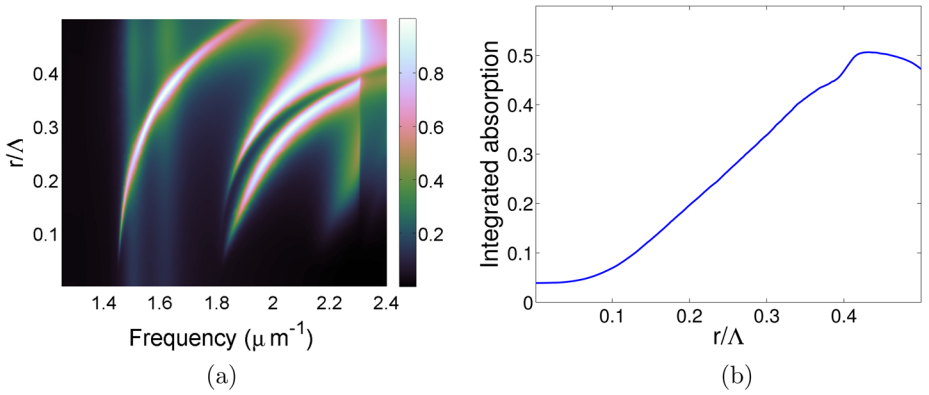

Figure 4. (a) Absorption as a function of frequency and hole radius r for a photonic crystal slab with fixed period Λ = 434 nm and thickness d = 95 nm. (b) Integrated absorption as a function of photonic crystal hole radius.

Figure 1b. (For reference, the integrated single-pass absorption above the band gap of MoS_2 is around 10%. We take the band gap energy as that of the lowest exciton transition, $\nu \approx 1.8$ eV, around 690 nm.) The photonic crystal slab is constructed of a high-index dielectric slab (Ta_2O_5, n = 2.1) with a square lattice of cylindrical air holes. We characterize the photonic crystal slab by its lattice constant Λ, the normalized hole radius r/Λ, and its thickness d. For the optimal design, we use Λ = 438 nm, r = 0.431Λ, and d = 97 nm.

Lattice Constant Variation. To maximize absorption at normal incidence, we want to *minimize* the number of free-space channels. Since the normal incidence wave can couple to the resonance, by reciprocity the resonance must be able to leak back into the normal direction as well, and hence diffraction at zero order will be present. On the other hand, any diffraction orders beside zero order represent an additional leakage mechanism for the resonance that reduces the resonant absorption enhancement. Therefore, we expect a lattice period that is subwavelength to most of the frequency band of interest. Here, we consider the visible regime, so λ_{min} = 400 nm and λ_{max} = 700 nm. Indeed, the optimal structure has a period of Λ = 438 nm. For a material with frequency-independent single-pass absorption, we would obviously choose $\Lambda < \lambda_{min}$. Due to the frequency-dependent absorption of MoS_2, we obtain the optimal frequency-integrated absorption with a period that is inside the frequency region of interest.

We show the absorption versus frequency and period Λ in Figure 3a, for thickness d = 95 nm and normalized radius r/Λ = 0.431. The vertical green stripes at frequencies of approximately 1.5 and 1.66 μm^{-1} correspond to the peaks in the MoS_2 single-pass absorption at the A and B exciton transitions.[30] The bright white and pink horizontal bands correspond to significant absorption enhancement via interaction with guided resonances. The absorption enhancement is strongest for 260 nm < Λ < 700 nm, just slightly broader than the wavelength range of interest. For periods with Λ > 700 nm, the diffraction losses become high, reducing the absorption enhancement. In contrast, when the grating period is much smaller than the wavelength, the slab begins to look like a homogeneous dielectric with an effective index. Therefore, for periods smaller than about 200 nm the absorption is a smooth function of frequency without any sharp peaks (area of Figure 3a below the white bands).

We show the integrated absorption as a function of Λ in Figure 3b. The integrated absorption reaches a maximum of 51% at Λ = 438 nm. Since we hold r/Λ constant, as we increase Λ both the hole radius and the distance between holes increase. When both of these quantities are larger than the wavelength, we expect a decrease in scattering efficiency. This accounts for the drop in absorption to the right of the peak in Figure 3b. For large Λ, the absorption flattens out to around 27%. For very small (large) periods, the feature size will be much smaller (larger) than a wavelength, and thus we can treat the structure as a homogeneous slab using effective medium theory. For r/Λ = 0.431, this gives a filling fraction of 0.416 for an effective index of n_{eff} = 1.42. This in turn yields an expected integrated absorption of about 26%, very close to the value observed for large periods.

Hole Radius Variation. Due to the requirement of operating in the overcoupling regime, we expect to use a large radius for the air holes, since in general the radiative leakage rates for the guided resonances of a photonic crystal slab increase with r. In Figure 4a we see the MoS_2 absorption as a function of frequency and hole radius r, for Λ = 434 nm, d = 95 nm. The absorption due to the A and B exciton transitions is again visible as the vertical green streaks at around 1.5 and 1.66 μm^{-1}. The three pink-white bands represent strong absorption due to interaction with the guided resonances. The resonances exhibit some blue shift as r increases, since the effective index of the slab decreases as r increases. In addition, the bands widen in frequency for larger air holes, which significantly broadens the bandwidth of the resonances, as expected since larger holes result in stronger out-of-plane scattering. The right edge of the figure, with frequencies above $1/\Lambda$ = 2.3 μm^{-1}, appears "grayed out". These frequencies have wavelengths shorter than the lattice constant ($\lambda < \Lambda$ = 434 nm), which allows light at these frequencies to be diffracted from the photonic crystal slab and propagate in air away from the normal direction. This opening of a second free-space channel leads to reduced absorption in this frequency range.

Figure 4b shows the integrated absorption versus r, for d and Λ fixed. There is a maximum for r = 0.431Λ. The monotonic rise in integrated absorption as the hole radius increases from zero is expected, since we will have the greatest absorption enhancement in the overcoupled regime, which requires large holes. For hole radii larger than the peak, we observe a monotonic decrease. This is also expected, since once we remove too much of the high-index dielectric, we expect the total energy storage in the slab to decrease, and hence the integrated absorption as well.

Slab Thickness Variation. Naively, one may assume that a thick slab will maximize light trapping, since there are more

DOI: 10.1021/acsphotonics.5b00510
ACS Photonics 2016, 3, 571−577

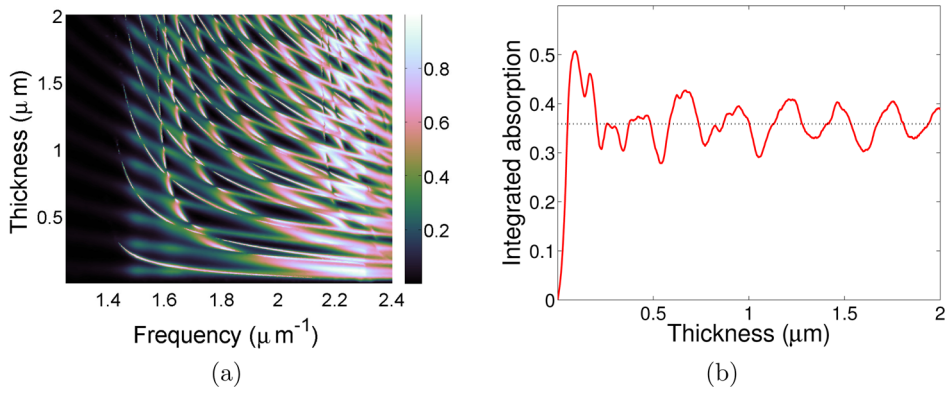

Figure 5. (a) Absorption as a function of frequency and photonic crystal slab thickness, for constant period Λ = 438 nm and hole radius $r = 0.431\Lambda$. (b) Integrated absorption as a function of photonic crystal slab thickness.

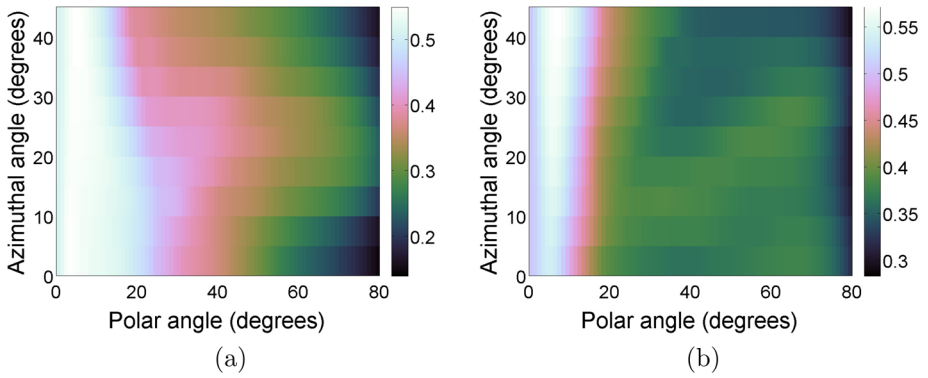

Figure 6. Frequency-integrated absorption as a function of angle for (a) p-polarization and (b) s-polarization.

guided resonances that the incident radiation can couple to. However, as the slab thickness increases, the modes become increasingly confined inside the slab and therefore have less overlap with the MoS_2 layer where the absorption occurs. As a result, for each mode the intrinsic dissipation rate γ_i decreases as the slab thickness increases. Furthermore, increasing the slab thickness will reduce the external leakage rate γ_e, so that we may no longer be operating in the overcoupling regime. In contrast, in the regime where the slab is very thin ($d \leq \lambda/4n$) the slab operates as a single-mode waveguide. While this reduces the number of modes M to unity, it maximizes the overlap between the single guided mode and the MoS_2. Furthermore, as the mode is less confined, we expect γ_e to be larger, ensuring that we operate in the overcoupling regime. For the optimal structure, the thickness is 95 nm, clearly in the single-mode regime.

Figure 5a shows absorption in the MoS_2 as frequency and the photonic crystal slab thickness d are varied. The pink-white bands indicate near-total absorption due to coupling to photonic crystal slab resonances, while the green bands (primarily visible in the lower left of the figure) represent absorption enhancement due to the Fabry–Perot background, as would also be observed by replacing the photonic crystal slab with a homogeneous dielectric slab. Consecutive Fano resonances are required to have opposite symmetry, unless there is a Fabry–Perot resonance between them. In this case, the Fano resonances will add constructively, which can lead to regions of broadband absorption that are nearly constant.[29] In the regions where the slab is thinner, these broad absorption bands tend to be flatter. Therefore, for a thin slab there will be only a few resonances, but they will each have a broad bandwidth, while for a thick slab there will be more resonances but they will each have a narrower bandwidth. Figure 5b shows the integrated absorption as a function of thickness for Λ = 438 nm, $r = 0.431\Lambda$. As the slab thickness goes to zero, integrated absorption goes smoothly to zero. We expect this since the mirror, which is assumed to be a perfect electric conductor, ensures that $E_{\parallel} = 0$ at its surface. As d increases, integrated absorption increases smoothly to an optimum at d = 95 nm. From there it reduces a bit and oscillates around a final value of about 35%. The oscillations arise from the competing processes of additional guided modes becoming available and the concomitant reduction in the mode overlap with the MoS_2 layer.

ANGULAR RESPONSE

We now examine the angular response of the structure. The frequency-integrated absorption as a function of polar angle θ, azimuthal angle ϕ, and polarization is shown in Figure 6. Approximately 30% of the sunlight that reaches Earth's surface is diffuse; we may treat this diffuse contribution as isotropic illumination spread over a hemisphere, with the incident intensity per solid angle constant. However, in order to calculate the angle-integrated intensity at a point, we must consider the incident flux. Thus, we calculate the angle-integrated absorption as

$$\bar{A} = \frac{\int_\phi d\phi \int_\theta d\theta A(\theta, \phi) \cos(\theta) \sin(\theta)}{\int_\phi d\phi \int_\theta d\theta \cos(\theta) \sin(\theta)} \quad (4)$$

DOI: 10.1021/acsphotonics.5b00510
ACS Photonics 2016, 3, 571–577

where the cos(θ) term arises since for a set of rays with angle of incidence θ the projected area of the solar cell to the plane perpendicular to the ray has a cos θ dependence, and the denominator allows us to assume a unit incident intensity.

As can be seen in Figure 6, the integrated intensity drops off with increasing polar angle for both polarizations and is largely independent of azimuthal angle. (Due to the symmetry of the structure, we need to study only the first 45° of azimuthal angle.) While the absorption drops off more quickly with polar angle for s-polarization, it remains higher overall (note the different lower limits of the two color bars). Over the frequency range of interest, the angle-integrated absorption was 0.355 for p-polarization and 0.382 for s-polarization. Therefore, the photonic crystal approach as discussed here can be used to achieve broadband absorption enhancement over a broad range of angles.

CONCLUSION

In conclusion, we have presented a simple geometry for optimized broadband absorption enhancement in monolayer MoS_2, with absorption surpassing the $4n^2$ limit at normal incidence. Through consideration of light trapping theory and parametric studies of the design parameters, we arrived at several design rules. First, we showed that the optimal photonic crystal slab has a grating period that is subwavelength to most of the frequency region of interest. This ensures that over most of the frequency range of interest diffraction orders above the directly transmitted zero order, which represent waves traveling away from the active layer that cannot be absorbed are eliminated. Second, the photonic crystal slab will have large air holes. The large holes will ensure that the guided mode resonances supported by the slab will be low-Q (high γ_e), ensuring that the device operates in the overcoupling regime. Finally, the optimal photonic crystal resonator will be thin. Using a thin slab ensures that the device operates in the single-mode regime, thereby increasing the overlap between the guided modes and the lossy layer. Furthermore, the thin slab leads to resonances with larger external leakage γ_e, again ensuring that the device operates in the overcoupling regime.

The geometry presented here is general and could be used with other TMDCs, such as WS_2 or WSe_2. In practice, the perfect electric conductor mirror could be replaced by a dielectric Bragg mirror, or a dielectric spacer could be added between the photonic crystal slab and a realistic metal mirror, in order to avoid parasitic losses in the metal. (For simplicity in illustrating the physics we have considered only a perfect electric conductor mirror in this article. However, we have also simulated the case where the perfect electric conductor mirror is replaced by a silver mirror separated from the photonic crystal by a dielectric spacer and observed similar broadband absorption enhancement in the MoS_2 layer.) While optimized for normal incidence light, the device also offers significant absorption enhancement for diffuse light as well. This geometry points directly toward a high-efficiency solar cell with nanometer-scale thickness.

MATERIALS AND METHODS

All calculations were performed with the S^4 implementation[31] of the rigorous coupled wave analysis algorithm.[32] The frequency-dependent complex permittivity of MoS_2 measured by Li et al. was used for the calculations.[30]

AUTHOR INFORMATION

Corresponding Authors

*E-mail: jpiper@exponent.com.

*E-mail: shanhui@stanford.edu.

Notes

The authors declare no competing financial interest.

ACKNOWLEDGMENTS

This work is supported in part by a Department of Energy Grant No. DE-FG07ER46426. J.R.P. is additionally supported by the Robert and Ruth Halperin Stanford Graduate Fellowship.

REFERENCES

(1) Novoselov, K. S.; Jiang, D.; Schedin, F.; Booth, T. J.; Khotkevich, V. V.; Morozov, S. V.; Geim, A. K. Two-dimensional atomic crystals. *Proc. Natl. Acad. Sci. U. S. A.* **2005**, *102*, 10451−3.

(2) Mak, K. F.; Lee, C.; Hone, J.; Shan, J.; Heinz, T. F. Atomically Thin MoS_{2}: A New Direct-Gap Semiconductor. *Phys. Rev. Lett.* **2010**, *105*, 136805.

(3) Splendiani, A.; Sun, L.; Zhang, Y.; Li, T.; Kim, J.; Chim, C.-Y.; Galli, G.; Wang, F. Emerging photoluminescence in monolayer MoS2. *Nano Lett.* **2010**, *10*, 1271−5.

(4) Wang, Q. H.; Kalantar-Zadeh, K.; Kis, A.; Coleman, J. N.; Strano, M. S. Electronics and optoelectronics of two-dimensional transition metal dichalcogenides. *Nat. Nanotechnol.* **2012**, *7*, 699−712.

(5) Sundaram, R. S.; Engel, M.; Lombardo, A.; Krupke, R.; Ferrari, A. C.; Avouris, P.; Steiner, M. Electroluminescence in single layer MoS2. *Nano Lett.* **2013**, *13*, 1416−21.

(6) Lopez-Sanchez, O.; Lembke, D.; Kayci, M.; Radenovic, A.; Kis, A. Ultrasensitive photodetectors based on monolayer MoS2. *Nat. Nanotechnol.* **2013**, *8*, 497−501.

(7) Zhang, W.; Chuu, C.-P.; Huang, J.-K.; Chen, C.-H.; Tsai, M.-L.; Chang, Y.-H.; Liang, C.-T.; Chen, Y.-Z.; Chueh, Y.-L.; He, J.-H.; Chou, M.-Y.; Li, L.-J. Ultrahigh-gain photodetectors based on atomically thin graphene-MoS2 heterostructures. *Sci. Rep.* **2014**, *4*, 3826.

(8) Pospischil, A.; Furchi, M. M.; Mueller, T. Solar-energy conversion and light emission in an atomic monolayer p-n diode. *Nat. Nanotechnol.* **2014**, *9*, 257−61.

(9) Ross, J. S.; Klement, P.; Jones, A. M.; Ghimire, N. J.; Yan, J.; Mandrus, D. G.; Taniguchi, T.; Watanabe, K.; Kitamura, K.; Yao, W.; Cobden, D. H.; Xu, X. Electrically tunable excitonic light-emitting diodes based on monolayer WSe2 p−n junctions. *Nat. Nanotechnol.* **2014**, *9*, 268−72.

(10) Wu, S.; Buckley, S.; Schaibley, J. R.; Feng, L.; Yan, J.; Mandrus, D. G.; Hatami, F.; Yao, W.; Vučković, J.; Majumdar, A.; Xu, X. Monolayer semiconductor nanocavity lasers with ultralow thresholds. *Nature* **2015**, *520*, 69−72.

(11) Gao, W.; Shu, J.; Qiu, C.; Xu, Q. Excitation of plasmonic waves in graphene by guided-mode resonances. *ACS Nano* **2012**, *6*, 7806−7813.

(12) Zhan, T. R.; Zhao, F. Y.; Hu, X. H.; Liu, X. H.; Zi, J. Band structure of plasmons and optical absorption enhancement in graphene on subwavelength dielectric gratings at infrared frequencies. *Phys. Rev. B: Condens. Matter Mater. Phys.* **2012**, *86*, 165416.

(13) Rybin, M. G.; Pozharov, A. S.; Chevalier, C.; Garrigues, M.; Seassal, C.; Peretti, R.; Jamois, C.; Viktorovitch, P.; Obraztsova, E. D. Enhanced optical absorbance of CVD-graphene monolayer by combination with photonic crystal slab. *Phys. Status Solidi B* **2012**, *249*, 2530−2533.

(14) Zhu, X.; Yan, W.; Uhd Jepsen, P.; Hansen, O.; Asger Mortensen, N.; Xiao, S. Experimental observation of plasmons in a graphene monolayer resting on a two-dimensional subwavelength silicon grating. *Appl. Phys. Lett.* **2013**, *102*, 131101.

(15) Gan, X.; Gao, Y.; Fai Mak, K.; Yao, X.; Shiue, R. J.; Van Der Zande, A.; Trusheim, M. E.; Hatami, F.; Heinz, T. F.; Hone, J.; Englund, D. Controlling the spontaneous emission rate of monolayer

DOI: 10.1021/acsphotonics.5b00510
ACS Photonics 2016, 3, 571−577

MoS2 in a photonic crystal nanocavity. *Appl. Phys. Lett.* **2013**, *103*, 2013−2016.
(16) Schwarz, S.; Dufferwiel, S.; Walker, P. M.; Withers, F.; Trichet, P.; Sich, M.; Li, F.; Chekhovich, E.; Borisenko, D. N.; Kolesnikov, N. N.; Novoselov, K. S.; Skolnick, M. S.; Smith, J. M.; Krizhanovskii, D. N.; Tartakovskii, a. I. Two-dimensional metal-chalcogenide films in tunable optical microcavities. *Nano Lett.* **2014**, *14*, 7003−7008.
(17) Wang, K. X.; Piper, J. R.; Fan, S. Optical impedance transformer for transparent conducting electrodes. *Nano Lett.* **2014**, *14*, 2755−8.
(18) Wu, S.; Buckley, S.; Jones, A. M.; Ross, J. S.; Ghimire, N. J.; Yan, J.; Mandrus, D. G.; Yao, W.; Hatami, F.; Vučković, J.; Majumdar, A.; Xu, X. Control of two-dimensional excitonic light emission via photonic crystal. *2D Mater.* **2014**, *1*, 011001.
(19) Lien, D.-h.; Kang, J. S.; Amani, M.; Chen, K.; Tosun, M.; Wang, H.-P.; Roy, T.; Eggleston, M. S.; Wu, M. C.; Dubey, M.; Lee, S.-C.; He, J.-h.; Javey, A. Engineering Light Outcoupling in 2D Materials. *Nano Lett.* **2015**, *15*, 1356−1361.
(20) Piper, J. R.; Fan, S. Total Absorption in a Graphene Monolayer in the Optical Regime by Critical Coupling with a Photonic Crystal Guided Resonance. *ACS Photonics* **2014**, *1*, 347−353.
(21) Piper, J. R.; Liu, V.; Fan, S. Total absorption by degenerate critical coupling. *Appl. Phys. Lett.* **2014**, *104*, 251110.
(22) Liu, Y.; Chadha, A.; Zhao, D.; Piper, J. R.; Jia, Y.; Shuai, Y.; Menon, L.; Yang, H.; Ma, Z.; Fan, S.; Xia, F.; Zhou, W. Approaching total absorption at near infrared in a large area monolayer graphene by critical coupling. *Appl. Phys. Lett.* **2014**, *105*, 181105.
(23) Brongersma, M. L.; Cui, Y.; Fan, S. Light management for photovoltaics using high-index nanostructures. *Nat. Mater.* **2014**, *13*, 451−60.
(24) Yu, Z.; Raman, A.; Fan, S. Fundamental limit of nanophotonic light trapping in solar cells. *Proc. Natl. Acad. Sci. U. S. A.* **2010**, *107*, 17491−6.
(25) Fan, S.; Joannopoulos, J. Analysis of guided resonances in photonic crystal slabs. *Phys. Rev. B: Condens. Matter Mater. Phys.* **2002**, *65*, 235112.
(26) Yu, Z.; Raman, A.; Fan, S. Thermodynamic Upper Bound on Broadband Light Coupling with Photonic Structures. *Phys. Rev. Lett.* **2012**, *109*, 173901.
(27) Yablonovitch, E. Statistical ray optics. *J. Opt. Soc. Am.* **1982**, *72*, 899.
(28) Stuart, H. R.; Hall, D. G. Thermodynamic limit to light trapping in thin planar structures. *J. Opt. Soc. Am. A* **1997**, *14*, 3001−3008.
(29) Sturmberg, B. C. P.; Dossou, K. B.; Botten, L. C.; McPhedran, R. C.; de Sterke, C. M. Fano resonances of dielectric gratings: symmetries and broadband filtering. *Opt. Express* **2015**, *23*, A1672−A1686.
(30) Li, Y.; Chernikov, A.; Zhang, X.; Rigosi, A.; Hill, H. M.; van der Zande, A. M.; Chenet, D. A.; Shih, E.-m.; Hone, J.; Heinz, T. F. Measurement of the optical dielectric function of monolayer transition-metal dichalcogenides: MoS2, MoSe2, WS2, and WSe2. *Phys. Rev. B: Condens. Matter Mater. Phys.* **2014**, *90*, 205422.
(31) Liu, V.; Fan, S. S4: A free electromagnetic solver for layered periodic structures. *Comput. Phys. Commun.* **2012**, *183*, 2233−2244.
(32) Moharam, M. G.; Gaylord, T. K. Rigorous coupled-wave analysis of planar-grating diffraction. *J. Opt. Soc. Am.* **1981**, *71*, 811−818.

DOI: 10.1021/acsphotonics.5b00510
ACS Photonics 2016, 3, 571−577